RSC Advances

PAPER

View Article Online
View Journal | View Issue

Cite this: *RSC Adv.*, 2014, **4**, 794

In situ growth of Rh nanoparticles with controlled sizes and dispersions on the cross-linked PVA–PEI nanofibers and their electrocatalytic properties towards H_2O_2†

Han Zhu,[a] Ming Zhang,*[ab] ShengYing Cai,[a] YingTing Cai,[a] Pan Wang,[a] ShiYong Bao,[a] MeiLing Zou[a] and MingLiang Du[ab]

Received 2nd September 2013
Accepted 8th November 2013

DOI: 10.1039/c3ra44834g

www.rsc.org/advances

A facile approach for the synthesis of uniform, small size and well-dispersed rhodium nanoparticles (RhNPs) on cross-linked polyvinyl alcohol–polyethyleneimine (PVA–PEI) nanofibers has been demonstrated. Various methods were firstly employed to cross-link PVA nanofibers and the cross-linked PVA–PEI nanofibers exhibited good water stability and porous structures after immersing in water for 72 h. Because of the strong chelate effects among the amine groups, hydroxyl groups and Rh^{3+} ions, uniform RhNPs with an average diameter of about 2.5 ± 0.2 nm can evenly and densely grow throughout the PVA–PEI nanofibers *via* an *in situ* reduction. Meanwhile, the better dispersion and smaller size of the RhNPs grown on the nanofibers in comparison with the pre-synthesized RhNPs directly deposited on the nanofibers exhibit the advantages of *in situ* reduction for size and dispersion control. The successful fabrication of the RhNPs/(PVA–PEI) nanofibers with various densities of well-dispersed RhNPs demonstrates that the strong chelate effects and stabilization of the PVA–PEI nanofibers also play an essential role in the size and dispersion control of RhNPs. The crystal structures, chemical bonding and interactions of the prepared nanofibers were verified using XPS and FTIR spectra and XRD patterns. These novel nanomaterials were fabricated as non-enzymatic electrochemical sensors and exhibit highly electrocatalytic activity towards H_2O_2.

Introduction

The rational design of new generation catalysts with excellent performance requires control over their architecture at the nanoscale. The size, shape and dispersion control of nanostructures determines their catalytic behavior through the adjustment of the number and geometric structure of the active sites.[1–3] Recently, noble metal nanoparticles (NPs) with sizes below 10 nm have been extensively studied in catalysis due to their high surface to volume ratios, unique electronic property and catalytic activity that are significantly different from their bulk forms.[4,5] To date, various noble metals, such as gold, silver, palladium, and platinum have been studied extensively in catalysis reactions.[6,7] However, compared to other noble metals, the synthesis of size-controlled and well-dispersed rhodium nanoparticles (RhNPs) is a challenging task and there are few reports on the size and dispersion control of RhNPs.[1,7] Rh is a choice metal for this study not only because of the lack of structural control but also because of its versatility, activity, and selectivity over so many chemical transformations, such as NO reduction, CO oxidation, hydrogenations, electro-oxidations, and hydroformylations.[8–12]

Previously literature has reported that the electrocatalytic activity of metal NPs is extremely sensitive to their sizes, shapes and dispersion.[13–15] Small size usually can dramatically affect their physical and chemical properties arise from their large surface-area-to-volume ratio and the spatial confinement of electrons, phonons, and electric fields in and around these particles.[16–19] However, along with the exciting properties caused by the small size, and due to the high surface energy and large surface curvature of NPs, significant challenges are still remain for the preparation and isolation of NPs with controlled sizes and dispersion.[1,2,20] The lack of the structural control for Rh could be attributed to the small number of suitable surfactants or adsorbate additives which can stabilize the growing Rh surface.[1] Therefore, the metal precursors are reduced in the presence of the surface stabilizer, which prevent aggregation and may also impact the control in the growth process. In addition, because of the growing environmental concerns and increasingly stringent regulations governing auto emissions,

[a]*Department of Materials Engineering, College of Materials and Textile, Zhejiang Sci-Tech University, Hangzhou 310018, P. R. China*

[b]*Key Laboratory of Advanced Textile Materials and Manufacturing Technology, Zhejiang Sci-Tech University, Ministry of Education, Hangzhou 310018, P. R. China. E-mail: du@zstu.edu.cn; Tel: +86-571-86843255*

† Electronic supplementary information (ESI) available. See DOI: 10.1039/c3ra44834g

more efficient, reproducible, stable catalysts are needed and based on the demands, more and more noble metal NPs are intend to load on the substrates.[15,21]

As a kind of 1-D substrates, polymer nanofibers prepared by the electrospinning process gradually attracted the attention of many researchers because of the associated advantages of the synthesizing technique and the obtained products.[22–25] Compared with the widely used 1-D substrates, such as carbon nanotubes, metal and metal oxide nanowires, the electrospun nanofibers possess several remarkable characteristics such as flexibility in surface functionalities, high specific surface area, high porosity and superior mechanical performance.[23–27] Meanwhile, the surfaces of the polymer nanofibers possess abundant chemical groups, making the polymer nanofibers to be optimal substrates for the immobilization of metal NPs. Among a wide series of electrospun polymers, poly(vinyl alcohol) (PVA) attracted particular attention due to its plenty advantageous properties such as water solubility, hydrophilicity, chemical and thermal stability, and biocompatibility.[24,28,29] However, the water soluble PVA nanofibers cannot stay in water, which impose restrictions on the widely practical applications. Various methods were employed to cross-liked PVA nanofibers using physical methods such as heat and radiation or chemical agents including glutaraldehyde (GA), glyoxal, and boric acid.[28,29] It should be noted that the cross-linkage of the PVA nanofibers usually results in the formation of merged and entangled nanofibers and the damages of the porous structures of the nanofibers.[20,30] Therefore, how to obtain the cross-linked PVA nanofibers with good water stability and porous structures still remain challenge.

Recent studies in our groups have shown that small, uniform and well-dispersed Au and AgNPs can be synthesized in polyacrylonitrile nanofibers or immobilized on the halloysite nanotubes *via in situ* reduction and these novel materials exhibit high catalytic activity and antibacterial property.[31–34] In addition, we also fabricated the sulfydryl functionalized water-stable PVA nanofibers to served as a nanoreactor for the *in situ* formation of AgNPs, and the fabricated AgNP-immobilized PVA nanofibers have been demonstrated to be a highly active biosensor for the detection of glutathione and glucose.[20,30] These successes in the fabrication of Au, Ag and PtNPs embedded in or immobilized on the electrospun polymer nanofibers lead us to develop a facile approach to synthesis small, uniform and well-dispersed RhNPs on the surfaces of cross-liked PVA nanofibers for the electrochemical detection of H_2O_2.

In the present investigations, various methods were firstly employed to cross-linked PVA nanofibers with good water stability and porous structures. The morphologies of cross-linked nanofibers immersed in water for the desired times help us to obtain a best substrates for the growth of RhNPs. The cross-linking reaction of PVA–PEI nanofibers is due to the formation of acetal bridges generated between PVA–GA, and aldimine linkages generated between the GA–PEI.[24,28–30] The chemical bondings informations were verified by the FTIR and XPS characterizations. The cross-linked PVA–PEI nanofibers with good water stability and porous structures were immersed in $RhCl_3$ solution to complex the Rh^{3+} ions with the amine and hydroxyl groups of the PEI–PVA nanofibers because of the chelate effects. Through the reduction by $NaBH_4$, small, uniform and well-dispersed RhNPs were grown on the surfaces of PVA–PEI nanofibers *via in situ* reduction. The pre-synthesized RhNPs in water directly deposited on the PVA–PEI nanofibers exhibit larger size and aggregated RhNPs clusters, indicating the advantages of the *in situ* reduction and the stabilization of the PVA–PEI nanofibers in the control of the size and dispersion of the RhNPs. A series of RhNPs/(PVA–PEI) nanofibers mats with various densities of RhNPs were prepared and the RhNPs can also show uniform size and well dispersion. The fabricated non-enzymatic RhNPs/(PVA–PEI) nanofibrous mats electrochemical sensors exhibit highly electrocatalytic activity towards H_2O_2, which would be the promising nanomaterials for the widely application in the biosensors and bioelectrocatalysis.

Experimental method

Materials

Rhodium (III) chloride hydrate ($RhCl_3 \cdot 3H_2O$, 99.9%), polyvinyl alcohol (88% hydrolyzed, $M_w = 88\,000$), and polyethyleneimine (PEI, branched, $M_w = 750\,000$, 50 wt% in water) were acquired from Shanghai Civi Chemical Technology Co., Ltd. Glutaraldehyde (GA) aqueous solution (30 wt%) and hydrochloric acid were obtained from Aladdin Chemistry Co., Ltd. Epigallocatechin gallate (EGCG) was purchased from Xuancheng Baicao Plant Industry and Trade Co., Ltd. Nafion aqueous solution (5 wt%) was obtained by Aldrich Chemistry Co., Ltd. All the chemicals were used as received without further purification. Deionized water (DIW, 18.2 MΩ) was used for all solution preparations.

Fabrication of the water-stable PVA nanofibrous mats *via* various methods

For the preparation of PVA solution (10 wt%), a certain amount of PVA powder was firstly dissolved in DIW at 85 °C overnight under magnetic stirring to get homogeneous solution, and then the solution was cooled down to room temperature naturally. (1) In the fabrication of PVA–GA nanofibers, the GA solution (30 wt%) was mixed with the PVA aqueous solution under vigorous stirring to achieve a homogeneous solution, in which the mass ratio of PVA and GA was 4 : 1. The prepared PVA–GA electrospun precursor solution was collected in a 10 mL syringe equipped with a 24 gauge stainless steel needle tip. The syringe was fixed on an electric syringe pump set to maintain constant feed rate of 0.01 mL min^{-1} for PVA–GA nanofibers. The voltage was 12 kV and the distance between the needle tip and the collector were 12 cm. (2) In the fabrication of the cross-linked PVA nanofibers, the PVA precursor solution (10 wt%) was firstly electrospun into the PVA nanofibers, and then treatment *via* the GA vapor in a vacuum oven at 60 °C for 24 h. (3) For the preparation of the acid promoted cross-linked PVA–GA nanofibers, the above prepared PVA–GA nanofibers were immersed in a mixed solution containing 10 vol% of HCl aqueous solution (37 wt%) and 90 vol% methanol for 24 h to produce water-stable nanofibrous mats. (4) For the preparation of PVA–PEI

electrospun precursor solution, PEI (50 wt%) and PVA (12 wt%) solutions were mixed together under magnetic stirring overnight with a PEI–PVA mass ratio of 1 : 3 to achieve a homogeneous solution. The electrospun procedure of PVA–PEI precursor was the same as PVA nanofibers. The constant of the feed rate, voltage and distance are 0.005 mL min^{-1}, 20 kV and 20 cm. The freshly prepared PEI–PVA nanofibers were then cross-linked by GA vapor to render the nanofibers with water stability. The diameters and distribution of all the prepared nanofibers were measured by Image-Pro Plus6.2 software (200 particles of nanofibers were randomly selected for the measurement).

Facile preparation of the RhNPs immobilized on cross-linked PVA–PEI nanofibers *via* an *in situ* reduction approach

0.110 g of the freshly prepared cross-linked PVA–PEI nanofibrous mats were immersed into the desired volume of $RhCl_3$ solution (5 mL, 10 mM) by vigorous shaking in an incubator shaker at room temperatures for 3 h to reach the adsorption equilibrium of the Rh^{3+} ions. Then the PVA–PEI nanofibers chelated with Rh^{3+} ions were rinsed with DIW and ethanol three times, respectively. After that, the prepared Rh^{3+}/(PVA–PEI) nanofibers mats were immersed into $NaBH_4$ solution followed by vigorous shaking in an incubator shaker at room temperatures for 1 h. The as-produced RhNPs/(PVA–PEI) nanofibers mats were rinsed with DIW three times, followed by drying at room temperature for 2 h, and stored under ambient conditions. The diameters and distribution of the RhNPs and nanofibers were measured by Image-Pro Plus6.2 software (200 particles of RhNPs were randomly selected for the measurement).

Fabrication of the RhNPs deposited on the cross-linked PVA–PEI nanofibrous mats

The RhNPs (5 mL, 10 mM) were firstly synthesized in DIW (45 mL) using $NaBH_4$ as the reductant and the EGCG as the stabilizer. Then, 0.110 g of the freshly prepared cross-linked PVA–PEI nanofibrous mats were immersed into the desired volume of RhNPs (50 mL) solution by vigorous shaking in an incubator shaker at room temperatures for 3 h to reach the adsorption equilibrium of the RhNPs. The as-produced RhNPs/(PVA–PEI) nanofibers mats were rinsed with DIW three times, followed by drying at room temperature for 2 h, and stored under ambient conditions. The diameters and distribution of the RhNPs and nanofibers were measured by Image-Pro Plus6.2 software (200 particles of RhNPs were randomly selected for the measurement).

Facile preparation of the RhNPs/(PVA–PEI) nanofibers with various loading of the RhNPs *via* an *in situ* reduction approach

A similar approach was used for the preparation of RhNPs/(PVA–PEI) nanofibers with various loading of the RhNPs. The PVA–PEI nanofibrous mats with same weight were immersed into DIW solution containing 1, 2.5, 5, 7.5 mL $RhCl_3$ solution, respectively, to reach the adsorption equilibrium of the Rh^{3+} ions. Then, the prepared Rh^{3+}/(PVA–PEI) nanofibers mats were immersed into $NaBH_4$ solution followed by vigorous shaking in an incubator shaker at room temperatures for 1 h. The as-produced RhNPs/(PVA–PEI) nanofibrous mats were rinsed with DIW three times, followed by drying at room temperature for 2 h, and stored under ambient conditions. The diameters and distribution of the RhNPs and nanofibers were measured by Image-Pro Plus6.2 software (200 particles of RhNPs were randomly selected for the measurement).

Electrocatalytic experiments

Electrocatalytic experiments were conducted with a CHI660C workstation (Shanghai Chenhua, Shanghai). All experiments were carried out using a conventional three-electrode system in 0.1 M phosphate buffered saline (PBS), where PVA–PEI/GCE and RhNPs/PVA–PEI/GCE was used as the working electrode, a platinum foil as the auxiliary electrode and a saturated Ag/AgCl electrode as the reference electrode. The buffer was purged with high-purity nitrogen for at least 30 min prior to each experiment, and the nitrogen environment was then kept over the solution to protect the solution from oxygen. Electrochemical performances of the fabricated electrodes were tested using a three-electrode system by cyclic voltammetry (CV).

Instrumentation

Transmission electron microscopy (TEM) images were obtained with a JSM-2100 transmission electron microscopy (JEOL, Japan) at an acceleration voltage of 200 kV. The EDS spectrum of the RhNPs/(PVA–PEI) nanofibers was also recorded by the TEM. The morphologies of all the electrospun nanofibers were observed by a JSM-6700F field-emission scanning electron microscope (FE-SEM, JEOL, Japan) at an acceleration voltage of 1 kV. X-ray Diffraction (XRD) patterns of the PVA–PEI nanofibers and RhNPs/(PVA–PEI) nanofibers were characterized with a SIEMENS Diffraktometer D5000 X-ray diffractometer using Cu K_α radiation source at 35 kV, with a scan rate of 0.02° 2θ s^{-1} in the 2θ range of 10–80°. Fourier transform infrared (FTIR) spectra were recorded on a Nicolet 5700 FTIR spectrometer in transmittance mode at a resolution of 4 cm^{-1} and 32 scans in the range from 4000 nm to 400 nm. Thermogravimetric analysis (TGA; Pyris 1) was carried out from 298 to 1073 K at a heating rate of 5 K min^{-1} in N_2 atmosphere. X-ray photoelectron spectra of cross-linked PVA–PEI nanofibers and RhNPs/(PVA–PEI) nanofibers were recorded using an X-ray Photoelectron Spectrometer (Kratos Axis Ultra DLD) with an aluminium (mono) K_α source (1486.6 eV). The aluminium K_α source was operated at 15 kV and 10 mA.

Result and discussion

A better substrate for the growth of RhNPs should be taken into account firstly. It is well-known that the PVA is one of the water-solubility polymer, and in the widely application, much attentions should be drawn to promote the water-stability of the PVA. In this paper, we used four different methods to prepare the cross-linked PVA nanofibers and the morphologies of the PVA

nanofibrous mats *via* different treatments before and after soaked in the water are shown in Fig. 1. Fig. 1a shows the PVA–GA nanofibrous mats prepared from the PVA–GA solution and smooth and uniform nanofibers with random orientation were obtained with an average diameter of 250 ± 38 nm (Fig. S1†). However, after soaking in water for 1 h, the reserved PVA nanofibers swell considerably and the nanofibers start to fuse with each other and destroy the porous structures. The control of the morphology and the porous structures of the nanofibrous mats is essential for the practical applications where a high surface-area-to-volume ratio is considered advantageous.[20,29] As shown in Fig. 1b, the cross-linked PVA nanofibers treated by GA vapor show distinct nanofibers with average diameter of 460 ± 54 nm (Fig. S2†). It can be observed from Fig. 2f that after soaking in the water for 24 h, the cross-linked PVA nanofibers were swollen, became soft, and intertwined together. Meanwhile, except for the destroyed porous structures, the morphology of the nanofibers still maintained in these mats, indicating that the GA vapor can indeed improve their water stability.

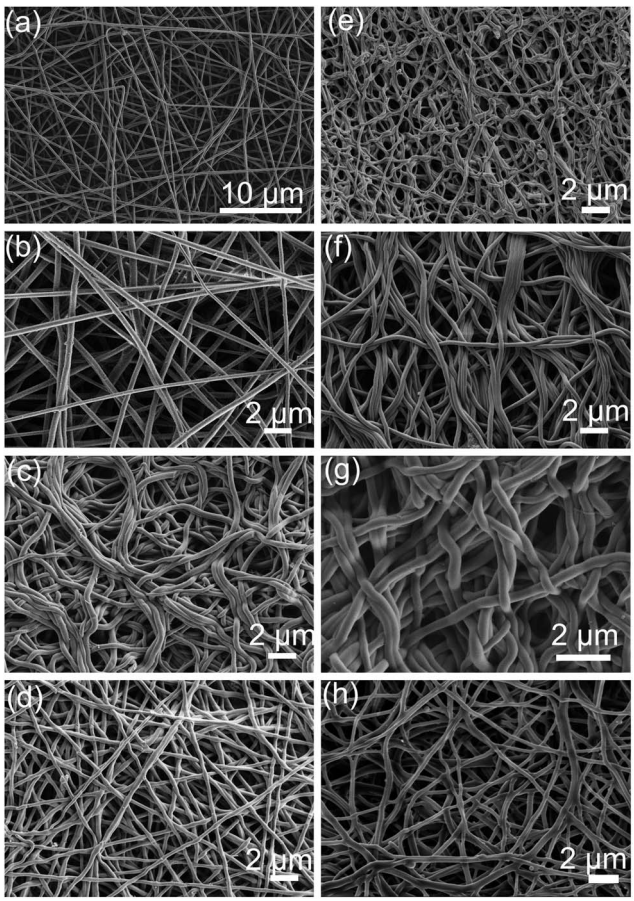

Fig. 1 FE-SEM images of the as-electrospun PVA–GA nanofibrous mats prepared from the PVA–GA mixed solution, (b) cross-linked PVA nanofibrous mats *via* GA vapor, (c) acid promoted GA cross-linked PVA–GA nanofibrous mats and (d) cross-linked PVA–PEI nanofibrous mats *via* GA vapor; FE-SEM images of the corresponding cross-linked PVA nanofibrous mats *via* different treatments immersed in water for (e) 1, (f) 24, (g) 48, and (h) 72 h, respectively.

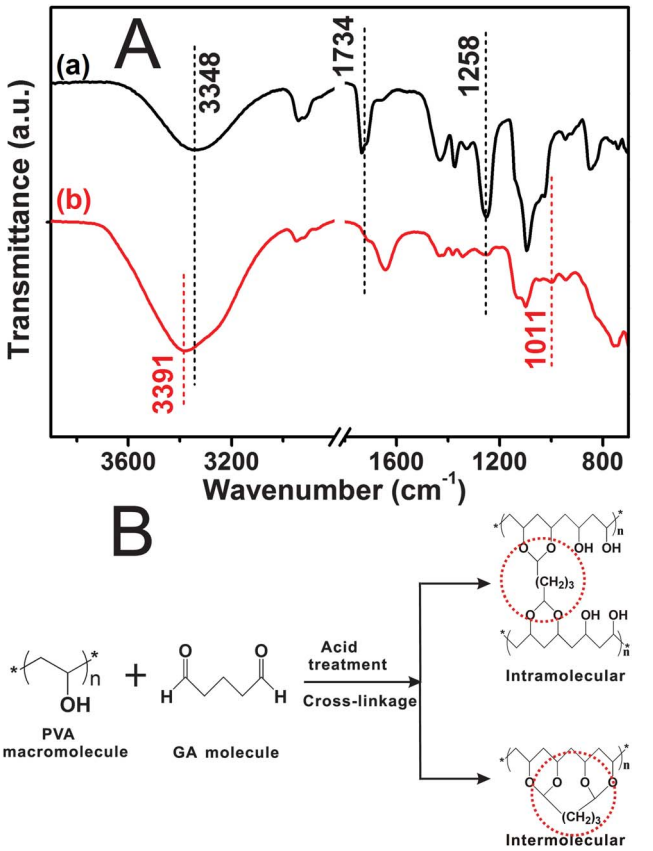

Fig. 2 (A) FTIR spectra of the (a) PVA–GA and (b) acid promoted cross-linked PVA nanofibrous mats; (B) schematic illustration of the cross-linkages between the hydroxyl groups of PVA and aldehyde groups of GA.

Fig. 1c shows the morphology of the acid promoted cross-linked PVA–GA nanofibrous mats. In a prepared procedure, the solution containing both PVA and GA was firstly electrospun into homogeneous nanofibers, and then the PVA–GA nanofibers were immersed into acidic solution to promote the cross-linking generated between hydroxyl groups of the PVA and the aldehyde groups of GA.[28,29] The morphology of the nanofibrous mats before and after immersing in water for 48 h did not change so much, indicating the enhanced water resistant compared with the freshly prepared PVA–GA nanofibers (Fig. 1a and b). However, the nanofibers before and after soaking in water were both merged and entangled among each other. Based on the above results, the simply mixed PVA with GA, GA vapor and acid promoted cross-linkage are not able to prepare the water-stable PVA nanofibers with uniform and distinct nanofibers, porous structures and high surface-area-to-volume ratio. Therefore, in order to keep the water stability along with the porous structures, another approach should be considered. In biomaterials and bioscience, the PEI polymer with perfect biocompatibility is widely used for the gene and drug delivery, gamma scintigraphy imaging agent, gene therapy and so on.[35–37] In the present investigation, we use the hyperbranched PEI polymer as the second component to promote the water-stability and morphology of the PVA nanofibers. The mixed PVA

and PEI solution were firstly electrospun into homogeneous nanofibers, and then treat *via* GA vapor for 24 h to improve the water-stability. As shown in Fig. 1d, uniform and distinct nanofibers with average diameter about 460 ± 52 nm (Fig. S3†) are observed, and the nanofibers only formed interfiber bonding/fused mostly at the intersection points because of the GA vapor. It is because that during the GA vapor procedure, the GA vapor contains water vapor and it can swell and soften the surface of the nanofibers, leading to the directly contact with nearby nanofibers at intersection points to form interfiber bonding.[29] After immersing in water for 72 h, there is almost no significant merged and entangled nanofibers and the porous structures still remains, indicating the reliable cross-linkage and good water-stability of PVA–PEI nanofibers. Compare the freshly cross-linked PVA–PEI nanofibers with the immersed nanofibers (480 ± 78 nm, Fig. S4†) for 72 h, the average diameters also did not change much.

The chemical bondings of the cross-linked PVA nanofibrous mats were confirmed by FTIR spectra. As shown in Fig. 2A, curve a shows the electrospun PVA–GA nanofibers prepared from the mixed PVA–GA solution, and the morphology of the nanofibers is corresponding to Fig. 1a. The broad band centered at 3348 cm^{-1} are associated with the stretching vibration of hydroxyl (–OH) groups from intermolecular and intramolecular hydrogen bonds.[20,28–30] The strong peaks located at 1734 and 1258 cm^{-1} are assigned to the C=O stretching vibration of free GA aldehyde groups and C–O stretching vibration of hydroxyl groups in PVA, respectively. The schematic illustration of the cross-linkages process between PVA and GA is shown in Fig. 2B. Compared with curve a, after the acid promoted cross-linkage of PVA–GA nanofibers, the intensities of the peaks at 1734 cm^{-1} and 1258 cm^{-1} decreased significantly. This means that the acid promoted the cross-linking of the aldehyde groups of GA and the hydroxyl groups of PVA, leading to the formation of ether linkages.[25] In addition, a new peak emerged at 1011 cm^{-1} is attributed to the formed ether linkages, indicating the formation of acetal bridges between the aldehyde and the hydroxyl groups. The cross-linkage both in intramolecular and/or intermolecular occurred within and at the point of contact nanofibers, leading to the phenomena of the merged and entangled nanofibers (Fig. 1c). The band became relative broad and moved to 3391 cm^{-1}, which also implied the involvement of the –OH groups in the cross-linkages, resulting in the partial destruction of hydrogen bonds.[30] The chemical bondings of the cross-linked PVA–PEI nanofibrous mats would discuss later.

Based on the above results, the cross-linked PVA–PEI nanofibers were used as the substrates for the growth of RhNPs. As shown in Fig. 3a, the FE-SEM image shows the distinct RhNPs/(PVA–PEI) nanofibers with uniformly average diameter of 540 ± 80 nm (Fig. S5†). The surfaces of the nanofibers are covered by large amounts of small RhNPs, which can also be observed by the TEM image (Fig. 3b). From Fig. 3c, a mass of RhNPs are evenly and densely distributed on the surface of the PVA–PEI nanofibers and there is nearly no aggregated RhNPs, indicating the strong stabilization of the amino and hydroxyl groups. A narrow diameter distribution of the RhNPs has been observed with an average size of 2.5 ± 0.2 nm (Fig. S6†) and the particle

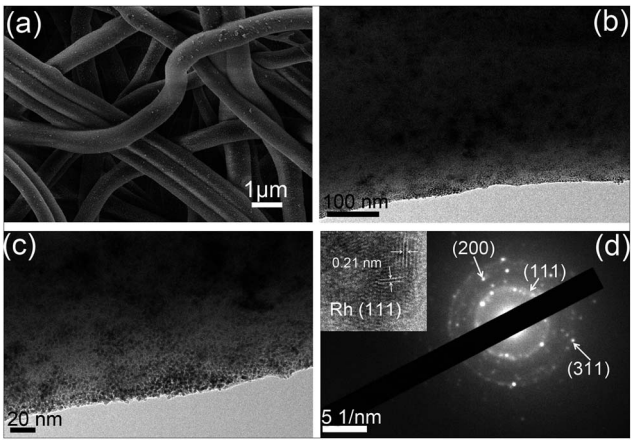

Fig. 3 FE-TEM (a) and TEM (b and c) images of the RhNPs/(PVA–PEI) nanofibers; SAED pattern of the RhNPs/PVA–PEI nanofibers and the inset is the HRTEM of the small RhNPs.

sizes were measured by 200 particles from enlarged TEM images using imaging analysis software, Image-Pro Plus6.2 software (Media Cybernetics Ltd). The size distribution diagram is shown in Fig. S6.† The inset in Fig. 3d exhibits a HRTEM image of RhNPs, showing lattice fringes of the (111) plane with an interplaner distance of 0.21 nm, which is according with the XRD results.[38–40] Fig. 3d shows the selected area electron diffraction (SAED) pattern of the RhNPs/(PVA–PEI) nanofibers and it reveals the polycrystal rings indexed to the (111), (200), and (311) planes of fcc Rh crystal, respectively, indicating the polycrystallinity of RhNPs.[39,41,42]

Because of the strong chelate effects among the –NH groups, –OH groups and Rh^{3+} ions, the small RhNPs can evenly grow on the surfaces of PVA–PEI nanofibers *via in situ* reduction, and the stabilization of PVA and PEI can impose restrictions on the size and distribution of RhNPs, leading to the formation of the uniform and well-dispersed RhNPs.[28,33,34] In order to show the advantages of the PVA–PEI assistant *in situ* reduction for the controlled size and distribution of RhNPs, we firstly synthesized the RhNPs by $NaBH_4$ in water and then the as-synthesized RhNPs were directly deposited on the PVA–PEI nanofibers. Fig. 4a shows the small and uniform RhNPs with average diameter of about 2.8 ± 0.3 nm (Fig. S7†), which is almost the same size as the RhNPs grown on PVA–PEI nanofibers (Fig. 3b). It is well known that because of the high surface energy, the RhNPs are easily aggregated to form larger sizes.[1,20] In our previously reports, a green compound, EGCG, was used both as reducer and stabilizer for the synthesis of AuNPs, PtNPs and AgNPs.[20,30,31]

In the present studies, with the assistant of the stabilization of the EGCG, there is no aggregated RhNPs in water (Fig. 4a and b). Fig. 4b shows the HRTEM image of RhNPs, the lattice fringes of an interplaner spacing of 0.21 nm is according with the (111) plane of RhNPs.[38–40] Compared with the *in situ* growth of RhNPs on PVA–PEI nanofibers (Fig. 3a), large size RhNPs clusters were deposited on the nanofibers, and the aggregated phenomena were relatively serious. As shown in Fig. 4d and e, the large size RhNPs clusters varied from 50 nm to 200 nm, are consist of

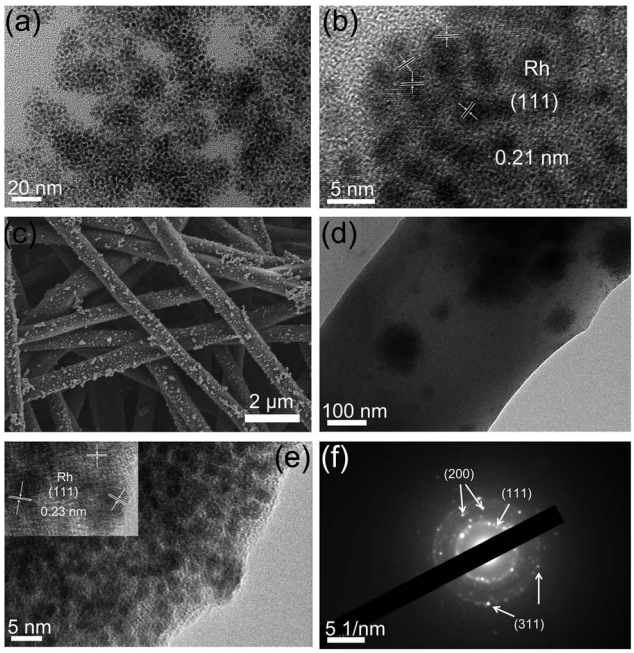

Fig. 4 (a) TEM and (b) HRTEM images of the synthesized RhNPs in water by $NaBH_4$ with the stabilization of EGCG; (c) FE-SEM and (d and e) TEM image and (f) SAED pattern of the PVA–PEI nanofibers deposited with RhNPs; the inset is the HRTEM image of the RhNPs deposited on PVA–PEI nanofibers.

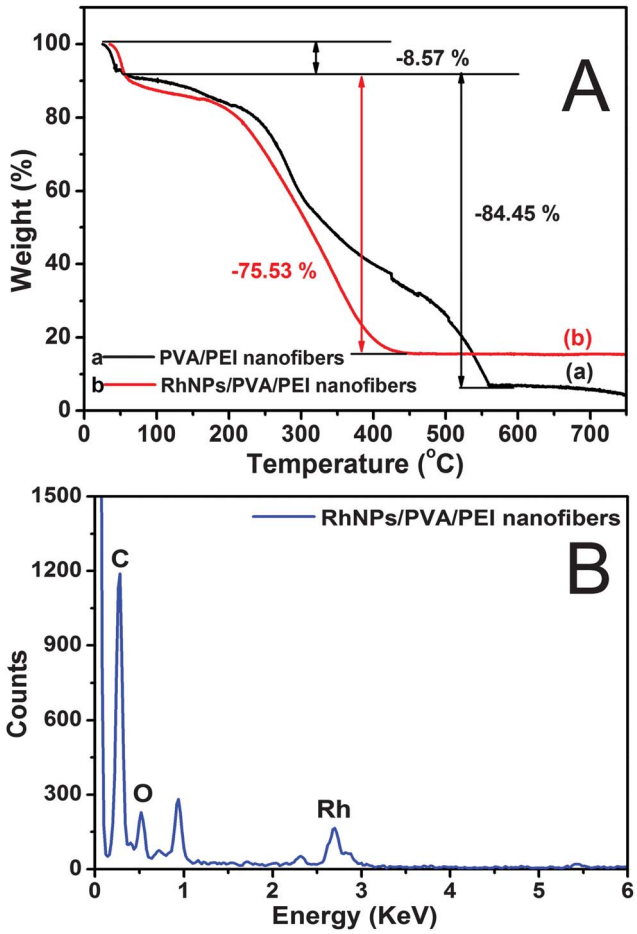

Fig. 5 (A) TGA curves of the cross-linked (a) PVA–PEI and (b) RhNPs/(PVA–PEI) nanofibers; (B) EDS spectra of the RhNPs/(PVA–PEI) nanofibers.

many small RhNPs. Small RhNPs are united to form Rh clusters, indicating that the –NH groups can not catch the small RhNPs to get a better distribution through the whole nanofibers. Therefore, the chelate effects between the NH groups and RhNPs is very weak, it cannot afford the enough stabilization for the RhNPs to prevent the aggregated RhNPs clusters. The inset in Fig. 4e show the lattice fringes of the Rh(111) planes, and the SAED pattern also reveals the polycrystal rings indexed to the (111), (200), and (311) planes of fcc Rh crystal, respectively, which are according with the XRD results.[39,41,42]

The results of thermogravimetric analysis (TGA) are displayed in Fig. 5A. The weight losses of 8.57 wt% for the cross-linked PVA–PEI and RhNPs/(PVA–PEI) nanofibers, are nearly both observed up to 55 °C, which can be attributed to the loss of free water molecular. The TGA curve of original cross-linked PVA–PEI nanofibers (curve a) shows that a great weight loss of 84.45 wt% occurred between 55 and 570 °C, which is caused by the decomposition of the PVA–PEI nanofibrous mats. Upon the temperature 570 °C, the polymer component of PVA–PEI nanofibrous mats was burned out. Compared with the curve a, the weight losses of 75.53 wt% for RhNPs/(PVA–PEI) nanofibrous mats is observed up to 450 °C, and the component of PVA–PEI nanofibrous mats have almost decomposed, while the Rh residues remains. With the comparison between the RhNPs/(PVA–PEI) nanofibrous mats and PVA–PEI nanofibrous mats, the loading capacity of RhNPs within the nanofibrous mats was estimated to be 8.92 wt%. Fig. 5B presents the results obtained from the energy dispersive X-ray spectroscopic (EDS) analysis. The EDS analysis was mostly used for the determination of elements present in the products. The EDS spectrum consisted of different peaks for Rh, C, and O. The large intense Rh peak came from the RhNPs, and the C and O peak came from the PVA, PEI and GA.

Fig. 6 shows the FTIR spectra of the pure PVA–PEI nanofibers and cross-linked PVA–PEI nanofibers with and without the growth of RhNPs. In the above discussion, the process and chemical bondings of cross-linkage between PVA and GA have been demonstrated. In this part, the hyperbranched PEI polymer possess large amounts of primary amine and imine groups with high activity and were used as the second component to crosslink the PVA nanofibers.[28,43,44] As shown in curve a and b, the peak located at 1650 cm^{-1} is ascribed to the bending vibrations of the primary amine groups in the pure and cross-linked PVA–PEI nanofibers, which is essential for the complexation of Rh^{3+} ions.[28] The strong peaks located at 1740 cm^{-1} and 1253 cm^{-1} are assigned to the C=O stretching vibration of aldehyde groups and the C–O stretching vibration of hydroxyl groups in PVA.[20,28,29] The peak located at the 1582 cm^{-1} is attributed to the bending vibration of imine groups in PEI.[45,46] After the treatment by GA vapor, some peaks have changed, which can identify the cross-linkage of the

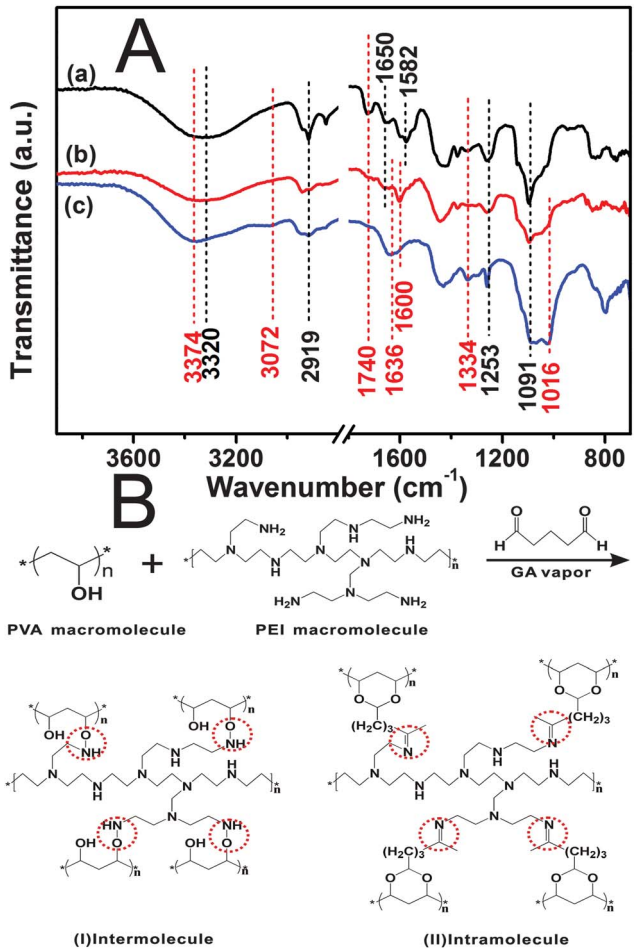

Fig. 6 FTIR spectra of the pure PVA–PEI (a), cross-linked PVA–PEI (b) and RhNPs/(PVA–PEI) (c) nanofibers; (B) schematic illustration of the cross-linkages between the PVA and PEI *via* the GA vapor.

PEI–PVA nanofibers. The peak ascribed to the C=O groups (1740 cm^{-1}) become weaker and a new peak emerged at 1600 cm^{-1} are indicative of the aldimine linkages generated between the GA–PEI.[28,29]

The chemical bondings among PVA, PEI and GA are shown in Fig. 6B. In addition, compared with curve a, another new peak located at 1016 cm^{-1} are emerged in curve b and c, and it belongs to the ether linkages generated between the GA–PVA. The above information can confirm the successful cross-linkage of the PVA–PEI nanofibers. The followed several evidences can support the chemical interactions among the amino groups, hydroxyls groups and RhNPs. After the growth of RhNPs on cross-linked PVA–PEI nanofibers, the peak location of primary amine groups (1650 cm^{-1}) moves to 1636 cm^{-1}, indicating the chemical interactions between the RhNPs and –NH groups. In addition, the peak ascribed to the bending vibration of amine groups becomes strong also can support the chelate effects. The broad band centered at 3320 cm^{-1} in curve a and b are attributed to the stretching vibrations of –NH and –OH groups, and with the growths of RhNPs, the peak moves to 3374 cm^{-1} and become relatively sharp, which is presumably due to the interaction between the amino/hydroxyl groups of the PEI–PVA polymers and the immobilized RhNPs.[30,31] Furthermore, as shown in curve c, two new peaks emerged at 3072 cm^{-1} and 1334 cm^{-1}, are attributed to the stretching and bending vibrations of associated –NH groups, respectively, which is caused by the hydrogen bonds and chelate effects.

Fig. 7 shows the morphology evolutions of the RhNPs/(PVA–PEI) nanofibers with various amounts of RhNPs. As shown in Fig. 7a, at the low concentration of $RhCl_3$, the as-formed RhNPs were well dispersed around the PVA–PEI nanofibers. With the increasing concentration of $RhCl_3$, more RhNPs were grown on the surfaces of the nanofibers and no obviously aggregated RhNPs clusters were observed, indicating the perfect stabilization of the PVA and PEI (Fig. 7b). When the amounts of $RhCl_3$ are further increased to 5 mL, more and more RhNPs formed on the surfaces of nanofibers until the nanofibers are completely encapsulated by a thin layer of RhNPs shells. In addition, there are still no significant aggregated RhNPs clusters. When 7.5 mL $RhCl_3$ adopted, large amounts of RhNPs are densely grown on the whole nanofibers, which are shown in Fig. 7d. Beyond the minimum loading of RhNPs, the RhNPs start to grow on the previously formed thin layer of RhNPs and join together to form a thicker solid RhNPs shells. Therefore, without the stabilization of the –NH and –OH groups of PVA–PEI nanofibers, more and more aggregated RhNPs clusters formed.

XRD patterns of the above RhNPs/(PVA–PEI) nanomaterials are shown in Fig. 8. As shown in Fig. 8, the curve a shows the XRD pattern of the pure PVA–PEI nanofibers and a broad peak centered at 20.8° is attributed to the (101) plane of semi-crystalline PVA.[47,48] XRD patterns of the RhNPs/(PVA–PEI) nanofibers with various amounts of $RhCl_3$ ranged from 1 mL to 7.5 mL are shown form curve b to curve e. When 1 mL $RhCl_3$ adopted, the as-prepared RhNPs/(PVA–PEI) nanofibers mats show very weak characteristic peaks of Rh crystal. With the amounts of $RhCl_3$ increase to 5 mL, three relatively distinct characteristic peaks of Rh crystal located at 40.2°, 49.7° and 70.0° can be observed, which are according with the (111), (200), and (220) planes ascribed to the face-centered cubic (fcc) Rh

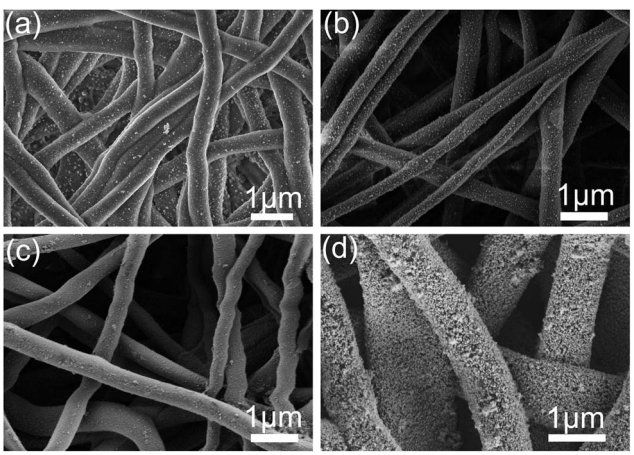

Fig. 7 FE-SEM images of the RhNPs/(PVA–PEI) nanofibers *via in situ* reduction with various amounts of $RhCl_3$ solution: (a) 1 mL, (b) 2.5 mL, (c) 5 mL and (d) 7.5 mL.

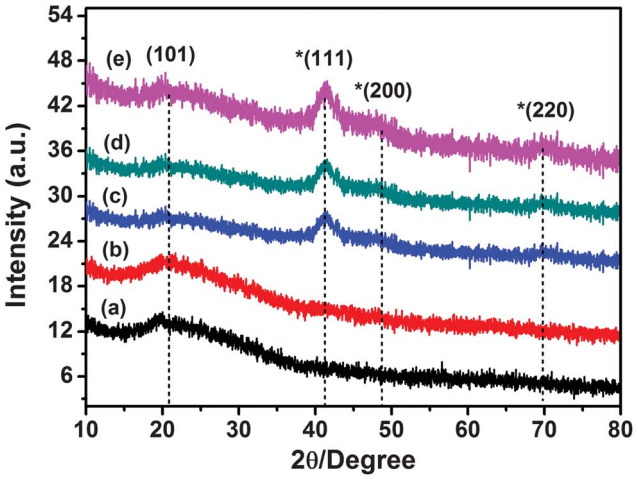

Fig. 8 XRD Patterns of the as-synthesized (a) PVA–PEI and RhNPs/(PVA–PEI) nanofibers with various amounts of $RhCl_3$ solution: (b) 1 mL, (c) 2.5 mL, (d) 5 mL and (e) 7.5 mL.

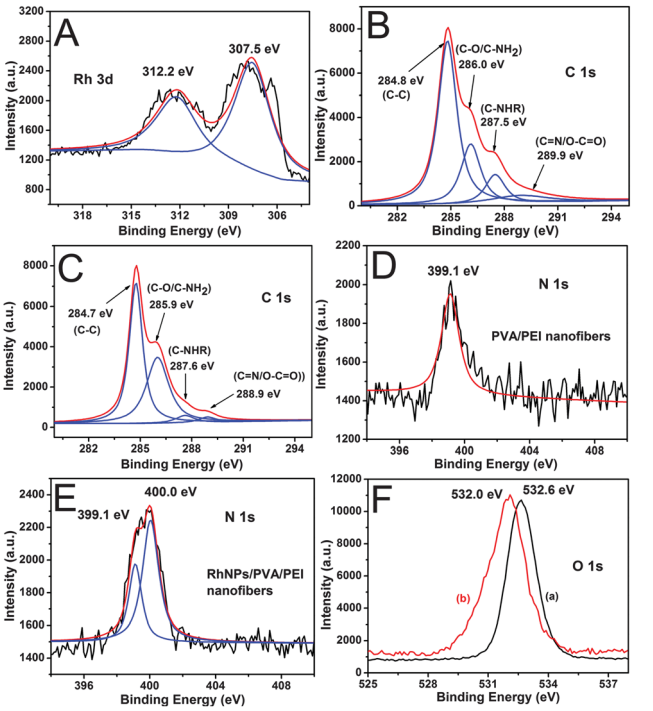

Fig. 9 (A) Rh 3d XPS spectra of the RhNPs/(PVA–PEI) nanofibrous mats; C 1s XPS spectra of the (B) cross-linked PVA–PEI nanofibers and (C) RhNPs/(PVA–PEI) nanofibers; N 1s XPS spectra of the (D) cross-linked PVA–PEI nanofibers and (E) RhNPs/(PVA–PEI) nanofibers; (F) O 1s XPS of the (a) cross-linked PVA–PEI nanofibers and (b) RhNPs/(PVA–PEI) nanofibers.

metal (JCPDS: 050685).[49–51] Although the XRD patterns of the PVA–PEI and RhNPs/(PVA–PEI) nanofibers look similar, close examination shows that because of the increased loading of RhNPs on PVA–PEI nanofibers, the relatively intensity of (101) plane peaks become weak, and while the intensity of the Rh plane peaks become strong. There is no other impurity peaks could be detected, such as Rh oxide, indicating the pure phase of the Rh nanocrystals. The XRD results also can shows several evidences for the stabilization effects to control the size of RhNPs. It is previously reported that the larger well faceted particles (>5 nm) have predominately exposed (111) crystal planes.[49] Grass *et al.* have prepared size-controlled RhNPs with average diameter ranged from 1.9 to 11.3 nm and study the size-depended XRD patterns.[49] If the size of RhNPs is lower than 5 nm, the (200) and (220) planes peaks are very weak, which are similar with the curve b, c and d. Therefore, based on the FE-SEM images and XRD patterns, the sizes of the major RhNPs grown on PVA–PEI nanofibers can be changed in the range from 2 to 6 nm (below 5 mL of the $RhCl_3$). The relative strong (111), (200) and (220) peaks (curve e) can also indicate the larger size of the RhNPs, which are due to the aggregated RhNPs clusters.

XPS spectra were used to testify the chemical states and chemical interactions of the prepared nanomaterials and help us to understand the growth process of the RhNPs on nanofibers. The whole XPS spectra of the PVA–PEI and RhNPs/(PVA–PEI) nanofibers are shown in Fig. S8.† Fig. 9A shows the Rh 3d core-level XPS spectra of the RhNPs/(PVA–PEI) nanofibers, and two peaks with binding energy (BE) at 307. 5 eV and 312.2 eV are consistent with the literature data for the BE of core levels Rh $3d_{5/2}$ and Rh $3d_{3/2}$, respectively, for the zero-valent Rh.[52–54] According to the literatures, the metallic Rh(0) shows $3d_{5/2}$ XPS signal at 307.2 eV, and the relative higher BE of RhNPs in PVA–PEI nanofibers are mainly attributed to the strong chemical bindings among the surface Rh atoms, NH groups and OH groups. The previously literatures have reported that the relatively high BE of metal NPs was due to the binding of surface metal atoms with the stabilizer or passive molecules surrounding the NPs, which lead to a substantial electron donation from metal NPs to the stabilizer molecules.[31] In addition, there are no additional peaks such as Rh(I) and Rh(III) appeared, suggesting that metallic Rh(0) is obviously the predominant species in the RhNPs.

As shown in Fig. 9B and C 1s XPS spectra of the cross-linked PVA–PEI nanofibers shows four significant peaks located at 284.8, 286.0, 287.5 and 289.9 eV, which are according with the carbon atoms in different functional groups: the C–C, the C in C–O and/or C–NH_2 bonds, the C in C–NHR bonds and the C in C=N (aldimine groups) and/or O–C=O bonds.[55–57] The existence of the aldimine groups indicate the cross-linkage of PVA–PEI nanofibers, which is according with the FTIR results. Compared with Fig. 9B, the C 1s XPS of the RhPNs/(PVA–PEI) nanofibers also shows four similar peaks, which are located at 284.7, 285.9, 287.6 and 288.9 eV, respectively. However, the intensity of the XPS peak of C–NHR bonds has a significant decrease after the growth of RhNPs, indicating the strong interactions between the NH groups and RhNPs. The N 1s XPS spectra of the PVA–PEI nanofibers shows a peak located at 399.1 eV (Fig. 9D), and after the growth of RhNPs, two obvious peaks are appeared in the N 1s XPS spectra of the RhNPs/(PVA–PEI) nanofibers (Fig. 9E). One of the peaks located at 399.1 eV belongs to the unchelated NH groups, while the BE of the other one moves to 400.0 eV because of the strong interactions between the NH groups and RhNPs.[33,57]

Meanwhile, the O 1s XPS spectra of the PVA–PEI nanofibers before and after the growth of RhNPs show two significant peaks, which are located at the 532.6 and 532.0 eV, respectively. The shift of the BE of O 1s can also indicate the strong interactions between the OH groups and RhNPs. Based on the XPS results for the O, N, C and Rh elements, it can be concluded that the chelating effects among the NH groups, OH groups and Rh^{3+} ions are the keys for the synthesis of uniform, small size and well dispersion RhNPs on PVA–PEI nanofibers. The schematic illustration of the growth process of the RhNPs on PVA–PEI nanofibers is shown in Scheme 1.

As shown in Scheme 1, the PVA–PEI nanofibers were firstly cross-linked by the GA vapor to improve the water stability of the nanofibrous mats. The surfaces of the PVA–PEI nanofibers possess abundant amino (NH) and hydroxyl (OH) groups and these groups can catch the Rh^{3+} ions to form chelate complex because of the chelate effects among the amino groups, hydroxyl groups and Rh^{3+} ions.[29–33] Then, the Rh^{3+}/(PVA–PEI) chelated nanofibers were immersed in the $NaBH_4$ solution, and because of the stabilization of the functional groups, the as-formed Rh chelate complexes were reduced to the small RhNPs immediately *via* the *in situ* reduction. The formed small RhNPs were immobilized on the surfaces of the nanofibers without any collision with other RhNPs. It means that the sizes and distributions of the RhNPs can be controlled through the chelate effects.

RhNPs possess distinct physical and chemical attributes that make them excellent scaffolds for the potential applications in electrocatalysis, electrochemical sensor, bioelectrocatalysis and so on.[58–60] The detection of H_2O_2 plays a significant role in many fields including clinic, food, pharmaceutical and environmental analyses.[20,28,61–63] The detection of H_2O_2 based on electrochemical sensors is one of the most used methods because of its low detection limit as well as low costs. However, most sensors based on enzymes or proteins may result in limited lifetime, stability problem and complex procedures in the fabrication process. Therefore, in the present investigation, the novel nanomaterials were used as a non-enzymatic electrochemical sensor for the electrocatalytic towards H_2O_2. The electrocatalytic activity of the as-prepared RhNPs/(PVA–PEI) nanofibers was studied with electrochemical cyclic voltammetry. Fig. 10A shows the cyclic voltammograms (CVs) of the (PVA–PEI)/GCE and RhNPs/(PVA–PEI)/GCE electrochemical sensors. Aqueous solutions with 1.0 mM of HQ in 0.1 M of sodium phosphate buffer (PB) at pH 6.8 were used for the electrochemical measurement. As shown in Fig. 10A, well-defined CVs of (PVA–PEI)/GCE (curve a) are observed, and the redox peak currents of HQ are about 28.6 and −16.6 μA, with potentials at 0.48 and 0.06 V, respectively.

For the RhNPs/(PVA–PEI)/GCE sensors (curve b and c), the intensities of redox peaks have an obvious increase, and the currents of HQ are about 52.7 and −28.4 μA, with potential at 0.48 and 0.00 V, respectively. The growth of RhNPs on PVA–PEI

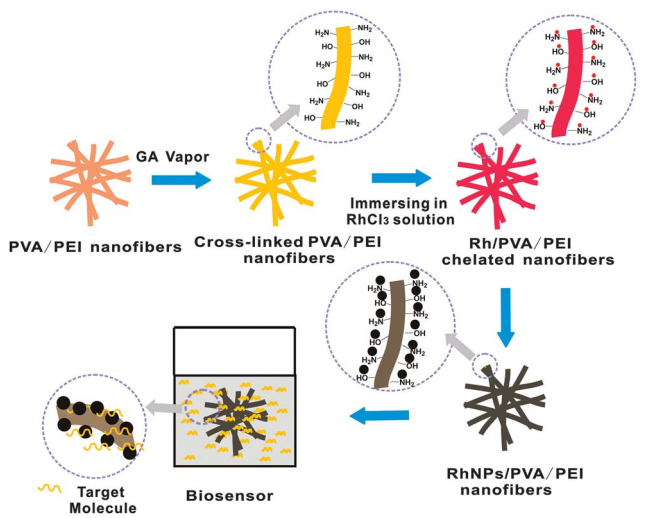

Scheme 1 Schematic illustration of the growth process of the RhNPs on PVA–PEI nanofibers and their application in electrochemical sensors for the electrocatalytic of H_2O_2.

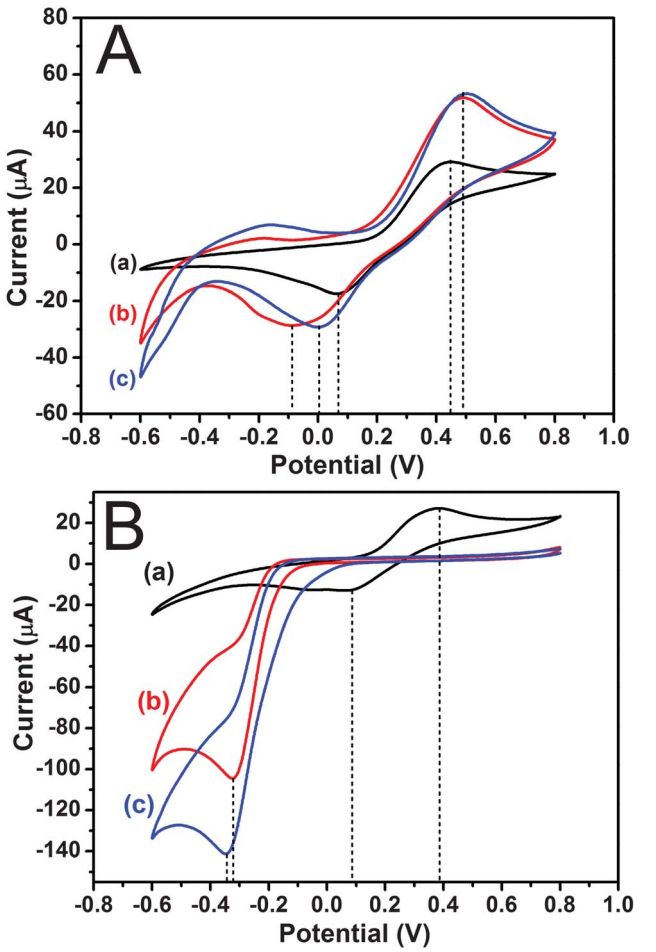

Fig. 10 (A) CVs of (a) PVA–PEI, (b) RhNPs/(PVA–PEI) (2.5 mL $RhCl_3$), and (c) RhNPs/(PVA–PEI) (5 mL $RhCl_3$) nanofibrous mats functionalized GCE with 1.0 mM HQ in 0.1 M PB (pH 6.8) (scan rate, 50 mV s^{-1}). (B) CVs of (a) PVA–PEI, (b) RhNPs/(PVA–PEI) (2.5 mL $RhCl_3$), and (c) RhNPs/(PVA–PEI) (5 mL $RhCl_3$) nanofibrous mats functionalized GCE with 1.0 mM HQ and 5.0 mM H_2O_2 in 0.1 M PB (pH 6.8) (scan rate, 50 mV s^{-1}).

nanofibers can improve the interfacial electron-transfer kinetics of HQ at the electrode interface, resulting in the increase of the currents.[20,28] As shown in Fig. 10B, with the addition of H_2O_2, the redox peak currents are about 27.5 and −12.4 μA, with potentials at 0.08 and 0.38 V. Compared with the currents of HQ obtained in Fig. 10A (curve a, 28.6 and −16.6 μA), the presence of H_2O_2 had little effects on the reduction peak currents (16.6 μA) and the potential of HQ (0.08 V), suggesting the weak reactions between HQ and H_2O_2. However, while for the RhNPs/(PVA–PEI) nanofibrous mats with various loading of RhNPs, with the addition of H_2O_2, the reduction peak currents (104 and 141 μA) caused by HQ both increased significantly accompanying with the disappearance of the oxidation current peak (Fig. 10B, curve b and c), indicating the strong reactions between H_2O_2 and HQ. In addition, compare curve b with curve c, the reduction peak currents increased from 104 μA to 141 μA with the increased loading of the RhNPs. The results indicate that the RhNPs/(PVA–PEI)/GCE electrochemical sensors exhibit remarkable electrochemical catalysis toward H_2O_2, indicating the fast direct electron transfer. Obviously, the presence of the small and well-dispersed RhNPs on PVA–PEI nanofibers is the key factor for the direct electron transfer, that is, the H_2O_2 molecule can fast and easily reach the surfaces of the RhNPs. Meanwhile, excellent electrocatalytic activity of the biosensors can also benefit from the highly porous fibrous structure and increased surface area of nanofibers mats. According to the previously studies,[20,30] the good peak currents can lead to the good current response towards the H_2O_2 and the peak currents obtained in this study are higher than our previously works at the same experimental conditions. The fabricated non-enzymatic RhNPs/(PVA–PEI) nanofibrous mats electrochemical sensor exhibit highly electrocatalytic activity towards H_2O_2, which would be the promising nanomaterials for the widely application in the biosensors and bioelectrocatalysis.

Conclusions

In summary, a facile approach to the synthesis of uniform, small sized and well-dispersed RhNPs on cross-linked PVA–PEI nanofibers has been demonstrated. In order to get a perfect substrate for the growth of RhNPs, various methods were firstly employed to cross-linked PVA nanofibers and the cross-linked PVA–PEI nanofibers show good water stability and porous structures after immersing in water for 72 h. The chemical bonding of the cross-linked PVA nanofibers was discussed and confirmed by XPS and FTIR spectra. Because of the strong chelate effects among the amine groups, hydroxyl groups and Rh^{3+} ions, uniform RhNPs with an average diameter of about 2.5 ± 0.2 nm can evenly and densely grow throughout the PVA–PEI nanofibers *via* an *in situ* reduction. Meanwhile, the better dispersion and smaller size of the RhNPs grown on the nanofibers in comparison with the pre-synthesized RhNPs directly deposited on the nanofibers exhibit the advantage of *in situ* reduction for the size and dispersion control. The successful fabrication of the RhNPs/(PVA–PEI) nanofibers with various densities of well-dispersed RhNPs (average diameter ranged from 2–6 nm) demonstrated that the strong chelate effects and stabilization of the PVA–PEI nanofibers play an essential factor for the size and dispersion control of RhNPs. The crystal structures and chemical interactions of the RhNPs/(PVA–PEI) nanofibers were verified by XPS spectra and XRD patterns. These novel nanomaterials were fabricated as non-enzymatic electrochemical sensors and exhibit highly electrocatalytic activity towards H_2O_2, which would be promising nanomaterials for wide application in biosensors and bioelectrocatalysis.

Acknowledgements

We acknowledge the support of the project of the National Natural Science Foundation of China (NSFC) (51243001, 51373154), the 521 Talent Project of Zhejiang Sci-Tech University, and Research Project of Department of Education of Zhejiang Province (Grant number: Y201122268).

Notes and references

1 B. T. Sneed, C. H. Kuo, C. N. Brodsky and C. K. Tsung, *J. Am. Chem. Soc.*, 2012, **134**, 18417.
2 D. A. J. M. Ligthart, R. A. Santen and E. J. M. Hensen, *Angew. Chem., Int. Ed.*, 2011, **50**, 5306–5310.
3 Z. L. Cheng, A. A. Zaki, J. Z. Hui, V. R. Muzykantov and A. Tsourkas, *Science*, 2012, **338**, 903–910.
4 J. A. Scholl, A. L. Koh and J. A. Dionne, *Nature*, 2012, **483**, 421–427.
5 S. B. Kim, R. D. Pike and D. A. Sweigart, *Acc. Chem. Res.*, 2013, **46**, DOI: 10.1021/ar300353n.
6 M. S. Hegde, G. Madras and K. C. Patil, *Acc. Chem. Res.*, 2009, **42**, 704–712.
7 H. B. Pan and C. M. Wai, *New J. Chem.*, 2011, **35**, 1649–1660.
8 H. Kobayashi, H. Morita, M. Yamauchi, R. Ikeda, H. Kitagawa, Y. Kubota, K. Kato, M. Takata, S. Toh and S. Matsumura, *J. Am. Chem. Soc.*, 2012, **134**, 12390.
9 H. Kobayashi, H. Morita, M. Yamauchi, R. Ikeda, H. Kitagawa, Y. Kubota, K. Kato and M. Takat, *J. Am. Chem. Soc.*, 2011, **133**, 11034.
10 S. Poorahong, P. Santhosh, G. V. Ramírez, T. F. Tseng, J. I. Wong, P. Kanatharana, P. Thavarungkul and J. Wang, *Biosens. Bioelectron.*, 2011, **26**, 3670–3673.
11 T. Ayvali, M. Zahmakıran and S. Ozkar, *Dalton Trans.*, 2011, **40**, 3584–3591.
12 H. Zhang, W. Y. Li, M. S. Jin, J. Zeng, T. Yu, D. Yang and Y. N. Xia, *Nano Lett.*, 2011, **11**, 898–903.
13 A. Fihri, M. Bouhrara, B. Nekoueishahraki, J. M. Basset and V. Polshettiwar, *Chem. Soc. Rev.*, 2011, **40**, 5181–5203.
14 N. T. Khi, J. S. Yoon, H. J. Kim, S. M. Lee, B. Kim, H. Baik, S. J. Kwon and K. Lee, *Nanoscale*, 2013, **5**, 5738–5742.
15 J. J. Hirner, Y. Shi and S. A. Blum, *Acc. Chem. Res.*, 2011, **44**, 603–613.
16 Y. Z. Lu and W. Chen, *ACS Catal.*, 2012, **2**, 84–90.
17 N. Dahal, S. Garcia, J. P. Zhou and S. M. Humphrey, *ACS Nano*, 2012, **6**, 9433–9446.

18 W. Y. Huang, J. N. Kuhn, C. K. Tsung, Y. W. Zhang, S. E. Habas, P. D. Yang and G. A. Somorjai, *Nano Lett.*, 2008, **8**, 2027–2034.
19 S. M. Humphrey, M. E. Grass, S. E. Habas, K. Niesz, G. A. Somorjai and T. Don Tilley, *Nano Lett.*, 2007, **7**, 785–790.
20 H. Zhu, M. L. Du, M. Zhang, P. Wang, S. Y. Bao, Y. Q. Fu and J. M. Yao, *Sens. Actuators, B*, 2013, **185**, 608–619.
21 B. Yoon and C. M. Wai, *J. Am. Chem. Soc.*, 2005, **127**, 17174–17175.
22 R. Sahay, P. S. Kumar, R. Sridhar, J. Sundaramurthy, J. Venugopal, S. G. Mhaisalkar and S. Ramakrishna, *J. Mater. Chem.*, 2012, **22**, 12953–12971.
23 D. Li and Y. N. Xia, *Adv. Mater.*, 2004, **16**, 1151–1170.
24 W. Y. Liu, S. Thomopoulos and Y. N. Xia, *Adv. Healthcare Mater.*, 2012, **1**, 10–25.
25 J. Wang, H. B. Yao, D. He, C. L. Zhang and S. H. Yu, *ACS Appl. Mater. Interfaces*, 2012, **4**, 1963–1971.
26 X. Fang, H. Ma, S. L. Xiao, M. W. Shen, R. Guo, X. Y. Cao and X. Y. Shi, *J. Mater. Chem.*, 2011, **21**, 4493–4501.
27 A. G. El-Deen, N. A. M. Barakat, K. A. Khalil and H. Y. Kim, *J. Mater. Chem. A*, 2013, **1**, 11001–11010.
28 Y. P. Huang, H. Ma, S. G. Wang, M. W. Shen, R. Guo, X. Y. Cao, M. F. Zhu and X. Y. Shi, *ACS Appl. Mater. Interfaces*, 2012, **4**, 3054–3061.
29 A. G. Destaye, C. K. Lin and C. K. Lee, *ACS Appl. Mater. Interfaces*, 2013, **5**, 4745–4752.
30 H. Zhu, M. L. Du, M. Zhang, P. Wang, S. Y. Bao, L. N. Wang, Y. Q. Fu and J. M. Yao, *Biosens. Bioelectron.*, 2013, **49**, 210–215.
31 H. Zhu, M. L. Du, M. L. Zou, C. S. Xu, N. Li and Y. Q. Fu, *J. Mater. Chem.*, 2012, **22**, 9301–9307.
32 M. L. Zou, M. L. Du, H. Zhu, C. S. Xu, N. Li and Y. Q. Fu, *Polym. Eng. Sci.*, 2013, **53**, 1099–1108.
33 H. Zhu, M. L. Du, M. L. Zou, C. S. Xu and Y. Q. Fu, *Dalton Trans.*, 2012, **41**, 10465–10471.
34 M. L. Zou, M. L. Du, H. Zhu, C. X. Xu and Y. Q. Fu, *J. Phys. D: Appl. Phys.*, 2012, **45**, 325302–325308.
35 T. B. Ren, L. Li, X. J. Cai, H. Q. Dong, S. M. Liu and Y. Y. Li, *Polym. Chem.*, 2012, **3**, 2561–2569.
36 H. Petersen, P. M. Fechner, D. Fischer and T. Kissel, *Macromolecules*, 2002, **35**, 6867–6874.
37 W. Y. Yuan, Z. S. Lu and C. M. Li, *J. Mater. Chem.*, 2012, **22**, 9351–9357.
38 S. Kundu, K. Wang and H. Liang, *J. Phys. Chem. C*, 2009, **113**, 18570–18577.
39 M. Pradhan, S. Sarkar, A. K. Sinha, M. Basu and T. Pal, *J. Phys. Chem. C*, 2010, **114**, 16129–16142.
40 Q. Yuan, Z. Y. Zhou, J. Zhuang and X. Wang, *Chem. Mater.*, 2010, **22**, 2395–2402.
41 J. Walter, S. Wakita, W. Boonchuduang and S. Hara, *J. Phys. Chem. B*, 2002, **106**, 8547–8554.
42 B. A. Kakade, S. Sahoo, S. B. Halligudi and V. K. Pillai, *J. Phys. Chem. C*, 2008, **112**, 13317–13319.
43 A. F. Thunemann, *Macromolecules*, 2000, **33**, 6878–6885.
44 M. S. A. Rahaman, L. Zhang, L. H. Cheng, X. H. Xu and H. L. Chen, *RSC Adv.*, 2012, **2**, 9165–9172.
45 Y. Zhang, J. M. Liu and X. P. Yan, *Anal. Chem.*, 2013, **85**, 228–234.
46 A. Lopez-Marzo, J. Pons and A. Merkoc, *J. Mater. Chem.*, 2012, **22**, 15326–15335.
47 J. S. Lin, Y. Liu, D. Y. Wang, Q. Qin and Y. Z. Wang, *Ind. Eng. Chem. Res.*, 2011, **50**, 9998–10005.
48 K. Das, D. Ray, N. R. Bandyopadhyay, A. Gupta, S. Sengupta, S. Sahoo, A. Mohanty and M. Misra, *Ind. Eng. Chem. Res.*, 2010, **49**, 2176–2185.
49 M. E. Grass, S. H. Joo, Y. W. Zhang and G. A. Somorjai, *J. Phys. Chem. C*, 2009, **113**, 8616–8623.
50 T. Ikeda, A. K. Xiong, T. Yoshinaga, K. Maeda, K. Domen and T. Teranishi, *J. Phys. Chem. C*, 2013, **117**, 2467–2473.
51 Y. W. Zhang, M. E. Grass, W. Y. Huang and G. A. Somorjai, *Langmuir*, 2010, **26**, 16463–16468.
52 I. Pis, V. Stetsovych, J. Mysliveccek, M. Kettner, M. Vondracek, F. Dvorak, D. Mazur, V. Matolin and V. Nehasil, *J. Phys. Chem. C*, 2013, **117**, 12679–12688.
53 A. Iordan, M. Zaki, C. Kappenstein and C. Geron, *Phys. Chem. Chem. Phys.*, 2003, **5**, 1708–1715.
54 Y. Wang, Y. G. Nie, J. S. Pan, L. K. Pan, Z. Sun, L. L. Wang and C. Q. Sun, *Phys. Chem. Chem. Phys.*, 2010, **12**, 2177–2182.
55 J. J. Yuan and R. H. Jin, *J. Mater. Chem.*, 2011, **21**, 10720–10729.
56 H. Y Liu, T. Kuila, N. H. Kim, B. C. Ku and J. H. Lee, *J. Mater. Chem. A*, 2013, **1**, 3739–3746.
57 E. P. Dillon, C. A. Crouse and A. R. Barron, *ACS Nano*, 2008, **2**, 156–164.
58 D. Astruc, E. Boisselier and C. Ornelas, *Chem. Rev.*, 2010, **110**, 1857–1959.
59 D. J. M. Snelders, N. Yan, W. J. Gan, G. Laurenczy and P. J. Dyson, *ACS Catal.*, 2012, **2**, 201–207.
60 J. Satija, V. V. R. Sai and S. Mukherji, *J. Mater. Chem.*, 2011, **21**, 14367–14386.
61 Y. Li, J. J. Zhang, J. Xuan, L. P. Jiang and J. J. Zhu, *Electrochem. Commun.*, 2010, **12**, 777–780.
62 K. J. Chen, K. C. Pillai, J. Rick, C. J. Pan, S. H. Wang, C. C. Liu and B. J. Hwang, *Biosens. Bioelectron.*, 2012, **33**, 120–127.
63 J. J. Wang, D. X. Han, X. H. Wang, B. Qi and M. S. Zhao, *Biosens. Bioelectron.*, 2012, **36**, 18–21.